Journal of Zhejiang University-SCIENCE C (Computers & Electronics)
ISSN 1869-1951 (Print); ISSN 1869-196X (Online)
www.zju.edu.cn/jzus; www.springerlink.com
E-mail: jzus@zju.edu.cn

Calculating the transient behavior of grounding systems using inverse Laplace transform

Nabiollah RAMEZANI[1], Seyed Mohammad SHAHRTASH[2]

([1]*Behshahr Branch, Iran University of Science and Technology, Behshahr 47137, Iran*)

([2]*Center of Excellence for Power Systems Automation and Operation, Department of Electrical Engineering, Iran University of Science and Technology, Tehran 16844, Iran*)

E-mail: {n_ramezani, shahrtash}@iust.ac.ir

Received Dec. 20, 2009; Revision accepted Apr. 12, 2010; Crosschecked Dec. 6, 2010

Abstract: This paper deals with a unified and novel approach for analyzing the frequency and time domain performance of grounding systems. The proposed procedure is based on solving the full set of Maxwell's equations in the frequency domain, and enables the exact computation of very near fields at the surface of the grounding grid, as well as far fields, by simple and accurate closed-form expressions for solving Sommerfeld integrals. In addition, the soil ionization is easily considered in the proposed method. The frequency domain responses are converted to the time domain by fast inverse Laplace transform. The results are validated and have shown acceptable accuracy.

Key words: Electromagnetic field, Near-field computation, High frequency performance, Soil ionization, Grounding system, Fast inverse Laplace transform

doi:10.1631/jzus.C0910777 **Document code:** A **CLC number:** O441.5

1 Introduction

Optimum performance of the grounding systems in substations is very important for providing human safety, correct operation of protective device, dissipation of lightning and fault currents, minimization of the flashovers during transients, electromagnetic compatibility in sensitive electrical equipments, and insulation coordination of power systems. The behavior of grounding systems in steady state (at power frequency) is well understood through many procedures proposed in the literature. But the high frequency analysis of grounding grids under impulse currents excited by lightning discharges, switching, and faults are still under research. For investigating the high frequency performance of grounding systems, many studies have been performed.

In general, high frequency modeling of grounding grids can be classified into four categories:

1. Circuit modeling (Meliopoulos and Moharam, 1983; Ramamoorty *et al.*, 1989; Geri *et al.*, 1992; Geri, 1999; Otero *et al.*, 1999; Cidras *et al.*, 2000), which is based on replacing all conductors of the grounding system by an equivalent circuit containing lumped capacitors, inductors, and resistors with too many approximations.

2. Electromagnetic field calculation methods (Grcev, 1986; Gao *et al.*, 2002; Lorentzou *et al.*, 2003; Arnautovski-Toseva and Grcev, 2004; Doric *et al.*, 2004; Poljak and Doric, 2006; Shahrtash and Ramezani, 2008), which solve the problem in time and frequency domains by using the full set of Maxwell's equations. These methods have made the least assumptions and are the most accurate procedures.

3. Hybrid methods (Heimbach and Grcev, 1997; Portela, 1997; Andolfato *et al.*, 2000; Zhang *et al.*, 2005), which combine the circuit and electromagnetic field approach. In these procedures, the analysis is more easily carried out compared with the electromagnetic field method, but with lower accuracy.

4. Equivalent transmission line substitution (Verma and Mukhedkar, 1980; Velazquez and Mukhedkar, 1984; Mentre and Grcev, 1994; Liu *et al*., 2001), which is based on traveling wave calculations. This model neglects the mutual electromagnetic coupling between grounding conductors and its accuracy is not as desirable.

In this paper, an accurate and simple procedure is presented based on the electromagnetic field theory to compute the high frequency response of buried grounding systems. The most important feature of the proposed method is that an accurate improved-image theory is used to solve the Sommerfeld half-space problem for the computation of far and near fields in any frequency.

In the proposed procedure, the transient problem is first solved by a formulation in the frequency or *s* domain. The grounding electrode is divided into small segments, where the length is chosen according to the minimum wavelength in the desired frequency spectrum. Then, at each frequency, on the basis of calculated leakage current distributions in these segments, the voltage at each pre-defined point is computed. Finally, the time domain transient responses are derived by applying a numerical fast inverse Laplace transform (FILT).

The main features of the proposed method are:

1. An exact modeling is proposed through the application of the full set of Maxwell's equations.

2. Closed-form relations are derived with high accuracy for near-field computations, considering the Sommerfeld integral for the air/earth interface contribution.

3. The frequency-dependent behavior of soil parameters is considered.

4. The effect of the soil ionization phenomenon is combined easily.

5. The problem is converted to *s*-domain and an FILT is applied to obtain time-domain results.

Finally, this method is implemented and compared with the methods in Grcev (1986), Doric *et al*. (2004), Poljak and Doric (2006), and Shahrtash and Ramezani (2008), which have similar approaches, but approximate procedures.

2 Frequency analysis of grounding electrode

In this work, the behavior of a grounding electrode is found in the frequency domain by computing the distribution of dissipated leakage currents from the electrode to earth and also its input impedance. Derivation of the relations and the whole procedure is described in the following sections.

2.1 Problem formulation

Fig. 1 shows a horizontal grounding electrode, which is a perfectly conducting element, with length L and radius r, buried in a lossy medium (earth) with permittivity ε_e, permeability μ_e, and conductivity σ_e, at depth H fed by a high frequency current source (I_s), which corresponds to lightning, faults, etc.

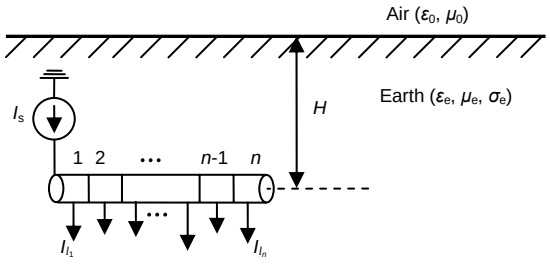

Fig. 1 Grounding electrode buried in earth

First, the grounding electrode is divided into n segments. To maintain high accuracy, the length of each segment should be less than one tenth of the minimum wavelength in the desired frequency spectrum.

Fig. 2 shows two sample segments of the grounding electrode. The normal electric field on the surface of the jth segment is the sum of $\boldsymbol{E}_{i_j}$ (the normal component of incident electric field intensity impressed by the high frequency source on the surface of this segment) and $\boldsymbol{E}_{S_j}$ (the normal scattered electric field intensity caused by the leakage currents of other segments of the grounding system). Note that in contrast to analyzing the performance of antennas in receiving mode, where there is an incident field propagated around the antenna, in grounding grid cases there is no such incident field; i.e., $\boldsymbol{E}_{i_j}=\boldsymbol{E}_{i_k}=\boldsymbol{0}$ (Fig. 2).

In general, there are two types of segments: one is the source segment, which is only one and its current is equal to the known current, I_s, and the other corresponds to all other segments (from 1 to n), where the leakage current must be calculated. Therefore, the scattered electric field intensity on the jth segment, $\boldsymbol{E}_{S_j}$, can be divided into $\boldsymbol{E}_{S_g}$ (the source component) and $\sum_{p=1}^{n}\boldsymbol{E}_{S_p}$ (the components due to other segments).

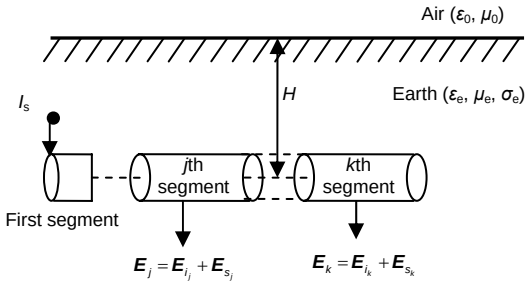

Fig. 2 Segments of grounding electrode impressed by electric fields

Assuming that the electric field at any point is known, the potential (U) caused by this electric field ($\boldsymbol{E}$) at any observation point (z) can be written as

$$U = -\int_{\infty}^{z} \boldsymbol{E}\cdot\boldsymbol{n}\,\mathrm{d}z\,, \tag{1}$$

where $\boldsymbol{n}$ is the unit vector normal to the surface of the conductor. For solving this problem, the normal boundary condition in the interface of the segments and the earth can be expressed as (McAllister and Crichton, 1991)

$$\boldsymbol{n}\cdot(\boldsymbol{D}_\mathrm{e} - \boldsymbol{D}_\mathrm{c}) = \delta_\mathrm{s}, \tag{2}$$

where $\boldsymbol{D}_\mathrm{e}$ and $\boldsymbol{D}_\mathrm{c}$ are the electric flux densities corresponding to the normal fields into the earth and at the boundary between conductors, respectively, and δ_s is the surface charge density on the conductor segments.

Also, according to the continuity equation in the time domain, the relation between the leakage current density ($\tilde{J}_\ell$) and the surface charge density is stated as (McAllister and Crichton, 1991)

$$\boldsymbol{n}\cdot\nabla\tilde{J}_\ell + \frac{\partial\delta_\mathrm{s}}{\partial t} = 0. \tag{3}$$

The first term in the left-hand side of Eq. (3) represents the normal divergence of $\tilde{J}_\ell$ and takes part in the frequency domain presentation of this equation as follows:

$$\boldsymbol{n}\cdot\frac{\mathrm{d}\boldsymbol{J}_\ell}{\mathrm{d}z} + \mathrm{j}\omega\delta_\mathrm{s} = 0, \tag{4}$$

where ω is the angular frequency.

According to Eqs. (2) and (4) and replacing $\boldsymbol{D}_\mathrm{e}=\varepsilon_\mathrm{e}\boldsymbol{E}$, $\boldsymbol{D}_\mathrm{c}=\varepsilon_\mathrm{c}\boldsymbol{E}_\mathrm{c}=\boldsymbol{0}$ (since the electric field intensity is zero inside the conductor), it can be concluded that

$$\boldsymbol{E}_{S_j\,\mathrm{normal}} = \frac{-1}{\mathrm{j}\omega\varepsilon_\mathrm{e}}\frac{\mathrm{d}\boldsymbol{J}_{\ell_j}}{\mathrm{d}z}. \tag{5}$$

Dividing the scattered electric field intensity into its components, Eq. (5) can be converted to

$$\begin{aligned}\int_{\infty}^{z}\left(\boldsymbol{E}_{S_g} + \sum_{p=1}^{n}\boldsymbol{E}_{S_p}\right)\cdot\boldsymbol{n}\,\mathrm{d}z &= \frac{-1}{\mathrm{j}\omega\varepsilon_\mathrm{e}}\boldsymbol{J}_{\ell_j}\cdot\boldsymbol{n}\\ \Rightarrow V_{S_j} + V_{\ell_j} &= \frac{1}{\mathrm{j}\omega\varepsilon_\mathrm{e}}J_{\ell_j}.\end{aligned} \tag{6}$$

The first component of the voltage, V_{S_j}, is the voltage induced on the jth segment due to the current source and is calculated by

$$V_{S_j} = Z_{S_j} I_\mathrm{s}\,, \tag{7}$$

where Z_{S_j} is the mutual impedance between the source and the jth segment.

The second component, V_{ℓ_j}, is the induced voltage due to the leakage currents of different segments and is calculated by

$$V_{\ell_j} = \sum_{k=1}^{n} V_{jk} = \sum_{k=1}^{n} Z_{jk} I_{\ell k}, \quad j = 1, 2, ..., n, \tag{8}$$

while Z_{jj} is the self-impedance of the jth segment and is equal to the ratio of V_{jj} (the voltage induced on the jth segment due to its own leakage current) to I_{ℓ_j}, and Z_{jk} is the mutual impedance between the jth and kth segments and equals the ratio of V_{jk} to I_{ℓ_k}.

Therefore, Eq. (6), which is the basic relation for calculating the voltages of different segments, is converted to the matrix form as

$$\boldsymbol{Z}\boldsymbol{I}_\ell - \frac{f(\ell)}{\mathrm{j}\omega\varepsilon_\mathrm{e}}\boldsymbol{I}_\ell = -\boldsymbol{Z}_\mathrm{s} I_\mathrm{s}, \tag{9}$$

where $\boldsymbol{Z}$ contains the self and mutual impedances between segments and $\boldsymbol{Z}_\mathrm{s}$ contains the mutual impedances between the source and segments. The vector $\boldsymbol{I}_\ell$ represents the unknown leakage currents, and $f(\ell)$ is the shape function, which is the leakage current distribution modeled in different ways, such as linear and/or triangular relation.

2.2 Voltage across any segment

For a buried electrode injecting a leakage current into a lossy medium, according to the Ampere-Maxwell law, the leakage current density in the time domain, $\tilde{J}_\ell$, is given through

$$\tilde{J}_\ell = \sigma_\mathrm{e}\tilde{E}_\mathrm{s} + \varepsilon_\mathrm{e}\frac{\partial \tilde{E}_\mathrm{s}}{\partial t}, \tag{10}$$

where $\tilde{E}_\mathrm{s}$ is the normal scattered electric field intensity in the time domain. In the frequency domain, Eq. (10) can be written as

$$\boldsymbol{E}_\mathrm{s} = \frac{1}{\sigma_\mathrm{e} + \mathrm{j}\omega\varepsilon_\mathrm{e}}\boldsymbol{J}_\ell . \tag{11}$$

In addition, the Faraday-Maxwell law defines the scattered electric field intensity, $\boldsymbol{E}_\mathrm{s}$, in the frequency domain at any point, by

$$\boldsymbol{E}_\mathrm{s} = -\mathrm{j}\omega\boldsymbol{A} - \nabla V, \tag{12}$$

where $\boldsymbol{A}$ is the magnetic vector potential and V is the scalar electric potential caused by the leakage currents. According to the relations in Appendix A, the magnetic vector potential can be substituted by

$$\boldsymbol{A} = \mu_\mathrm{e}\boldsymbol{J}_\mathrm{e}(\nu), \tag{13}$$

where $\boldsymbol{J}_\mathrm{e}(\nu)$ is the volume density of the leakage current as defined by Eq. (B1). By using Eqs. (11)–(13), the voltage at any point, with distance r (in the air or earth), can be expressed by the following relation (refer to Appendix B):

$$V(r,\omega) = \frac{I_\ell}{4\pi}\left(\frac{1}{\sigma_\mathrm{e} + \mathrm{j}\omega\varepsilon_\mathrm{e}} + \mathrm{j}\omega\mu_\mathrm{e}\right)\cdot\int_{\ell_n} f(\ell)G(r)\,\mathrm{d}\ell, \tag{14}$$

where $G(r)$ is the Green function for half-space conducting medium and is described in Eqs. (19) to (29). Obviously, by the above relation and substituting the distance between the observation point and the source point in the Green function, i.e., $G(r_\mathrm{s})$, the first component of voltage in Eq. (6) can be calculated. Also, the second component of the voltage in Eq. (6) can be found by substituting the distance between the observation point and the considered segments in $G(r)$.

Moreover, by using Eq. (14), the average induced voltage on the jth segment caused by the leakage current of the ith segment can be written as

$$V_{\ell_j}(\mathrm{j}\omega) = \frac{I_{\ell_i}}{4\pi}\left(\frac{1}{\sigma_\mathrm{e} + \mathrm{j}\omega\varepsilon_\mathrm{e}} + \mathrm{j}\omega\mu_\mathrm{e}\right) \cdot\int_{\ell_j} f_j(\ell_j)\left[\int_{\ell_i} f_i(\ell_i)G(r_{ij})\mathrm{d}\ell_i\right]\mathrm{d}\ell_j, \tag{15}$$

and the average induced voltage on the jth segment caused by the source can be expressed as

$$V_{S_j} = \frac{1}{4\pi}\left(\frac{1}{\sigma_\mathrm{e} + \mathrm{j}\omega\varepsilon_\mathrm{e}} + \mathrm{j}\omega\mu_\mathrm{e}\right)\cdot\int_{\ell_j} f_j(\ell_j)G(r_{S_j})\mathrm{d}\ell_j. \tag{16}$$

2.3 Computation of matrix $\boldsymbol{Z}$

According to Eq. (15), the elements of matrix $\boldsymbol{Z}$ in Eq. (9) are calculated through

$$Z_{ji}(\mathrm{j}\omega) = \frac{V_{\ell_j}}{I_{\ell_i}} = \frac{1}{4\pi}\left(\frac{1}{\sigma_\mathrm{e} + \mathrm{j}\omega\varepsilon_\mathrm{e}} + \mathrm{j}\omega\mu_\mathrm{e}\right) \cdot\int_{\ell_j} f_j(\ell_j)\left[\int_{\ell_i} f_i(\ell_i)G(r_{ij})\mathrm{d}\ell_i\right]\mathrm{d}\ell_j, \tag{17}$$

where $f_i(\ell_i)$ and $f_j(\ell_j)$ are the shape functions for the ith and jth segments, respectively. r_{ij} is the distance between the middle point of the ith segment and the similar point on the outer surface of the jth segment, and r_{ii} equals the radius of the grounding electrode.

2.4 Computation of vector $\boldsymbol{Z}_\mathrm{s}$

According to Eq. (16), the elements of $\boldsymbol{Z}_\mathrm{s}$ in Eq. (9) are calculated through the following relation:

$$Z_{S_j} = \frac{V_{S_j}}{I_\mathrm{s}(\mathrm{j}\omega)} = \frac{1}{4\pi}\left(\frac{1}{\sigma_\mathrm{e} + \mathrm{j}\omega\varepsilon_\mathrm{e}} + \mathrm{j}\omega\mu_\mathrm{e}\right)\int_{\ell_j} f_j(\ell_j)G(r_{S_j})\mathrm{d}\ell_j, \tag{18}$$

where r_{S_j} is the distance of the middle point on the outer surface of the jth segment from the source (which is assumed as a point segment), and $I_\mathrm{s}(\mathrm{j}\omega)$ is the current source representation in the frequency domain.

2.5 Proposed method for computation of *G*(*r*)

In this subsection, the procedure of computing the Green function is explained. The method is simple and valid for calculating both near and far fields with enough accuracy under both conditions.

The formulas in Appendix C are applicable in calculating the Green function when an electrode is located above the ground. In the case of a grounding electrode, which is buried into the earth, however, the positions of the source and its image are changed (Fig. 3). Therefore, it is the lossy medium into which the current dipole is placed.

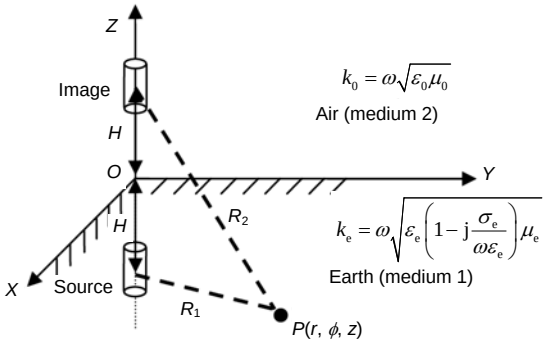

Fig. 3 Vertical dipole buried in the ground

Consequently, for a vertical dipole buried in the earth, the relations for the Green function are rewritten, changing the associated parameters of the two media (i.e., air and earth). Thus, the Green function, for this case, can be written as

$$G(r)=\int_0^\infty J_0(\lambda r)\mathrm{e}^{-q_\mathrm{e}(z-H)}\frac{\lambda\,\mathrm{d}\lambda}{\mathrm{j}q_\mathrm{e}}+\int_0^\infty\frac{q_\mathrm{e}-n^2q_0}{q_\mathrm{e}+n^2q_0}J_0(\lambda r)\mathrm{e}^{-\mathrm{j}q_\mathrm{e}(z+H)}\frac{\lambda\,\mathrm{d}\lambda}{\mathrm{j}q_\mathrm{e}},\tag{19}$$

where $q_0^2=k_0^2-\lambda^2$ and $q_\mathrm{e}^2=k_\mathrm{e}^2-\lambda^2$.

To reveal the contribution of the air/earth interface in Eq. (19), the following approach is carried out:

$$G(r)=\int_0^\infty J_0(\lambda r)\mathrm{e}^{-q_\mathrm{e}(z-H)}\frac{\lambda\,\mathrm{d}\lambda}{\mathrm{j}q_\mathrm{e}}+\int_0^\infty\left(\frac{q_\mathrm{e}-n^2q_0}{q_\mathrm{e}+n^2q_0}-1+1\right)J_0(\lambda r)\mathrm{e}^{-\mathrm{j}q_\mathrm{e}(z+H)}\frac{\lambda\,\mathrm{d}\lambda}{\mathrm{j}q_\mathrm{e}},\tag{20}$$

or

$$G(r)=\int_0^\infty J_0(\lambda r)\mathrm{e}^{-q_\mathrm{e}(z-H)}\frac{\lambda\,\mathrm{d}\lambda}{\mathrm{j}q_\mathrm{e}}+\int_0^\infty J_0(\lambda r)\mathrm{e}^{-q_\mathrm{e}(z+H)}\frac{\lambda\,\mathrm{d}\lambda}{\mathrm{j}q_\mathrm{e}}+\int_0^\infty\left(\frac{q_\mathrm{e}-n^2q_0}{q_\mathrm{e}+n^2q_0}-1\right)J_0(\lambda r)\mathrm{e}^{-\mathrm{j}q_\mathrm{e}(z+H)}\frac{\lambda\,\mathrm{d}\lambda}{\mathrm{j}q_\mathrm{e}}.\tag{21}$$

According to Ishimaru (1991), the first term of Eq. (21) is the Green function between the buried dipole and the observation point in the cylindrical coordinate system and equals the first term in the following Eq. (22) in the spherical coordinate system. In addition, the second term of Eq. (21) represents the Green function from the image of that dipole to the observation point, and is converted to the second term in Eq. (22) in the spherical coordinate system. Therefore, Eq. (21) takes the following form:

$$G(r)=\frac{\mathrm{e}^{-\mathrm{j}k_\mathrm{e}R_1}}{R_1}+\frac{\mathrm{e}^{-\mathrm{j}k_\mathrm{e}R_2}}{R_2}+\int_0^\infty\left(\frac{q_\mathrm{e}-n^2q_0}{q_\mathrm{e}+n^2q_0}-1\right)J_0(\lambda r)\mathrm{e}^{-\mathrm{j}q_\mathrm{e}(z+H)}\frac{\lambda\,\mathrm{d}\lambda}{\mathrm{j}q_\mathrm{e}}.\tag{22}$$

The third term of the Green function in Eq. (22), which stands for the air/earth interface contribution, is introduced as a correction term, ΔG_e, i.e.,

$$\Delta G_\mathrm{e}=\int_0^\infty f_\mathrm{e}(\lambda)J_0(\lambda r)\mathrm{e}^{-\mathrm{j}q_\mathrm{e}(z+H)}\mathrm{d}\lambda,\tag{23}$$

where

$$f_\mathrm{e}(\lambda)=-\frac{2n^2q_0}{n^2q_0+q_\mathrm{e}}\cdot\frac{\lambda}{\mathrm{j}q_\mathrm{e}}.\tag{24}$$

The integral in the right-hand side of Eq. (23) is a Sommerfeld type integral (SI) and is valid for the high frequency analysis of grounding systems, even where the observation point is in the vicinity of the grounding system. Since performing the analytical solution for these infinite integrals is much rigorous and rather time-consuming, much attention has been focused on developing numerical and approximate techniques for this problem.

Defining $n=k_\mathrm{e}/k_0$, Eq. (24) can be converted to

$$f_\mathrm{e}(\lambda)=-\frac{2k_\mathrm{e}^2q_0}{k_\mathrm{e}^2q_0+k_0^2q_\mathrm{e}}\cdot\frac{\lambda}{\mathrm{j}q_\mathrm{e}}.\tag{25}$$

As shown in Fig. 4, the integrand in Eq. (23) has two branch-points at $\lambda=k_0$ and $\lambda=k_e$. Due to the existence of a decreasing exponential factor depending on q_e in ΔG_e, the contribution of the point $\lambda=k_0$ to the integrand is smaller than the contribution of the point $\lambda=k_e$. Therefore, by substituting $q_0\approx k_0$ and $q_e\approx k_e$, Eq. (25) becomes

$$\begin{aligned} f_e(\lambda) &= -\frac{2k_e^2 q_0}{\frac{k_e^2}{k_0^2}\cdot\frac{k_0^2}{k_e^2}+1}\frac{\lambda}{\mathrm{j}k_0^2 q_e^2} \\ &\approx -\frac{2k_e^2 k_0}{n^2\cdot\frac{1}{n}+1}\frac{\lambda}{\mathrm{j}k_0^2 q_e^2} \Rightarrow f_e(\lambda)\approx\frac{2\mathrm{j}nk_e}{n+1}\frac{\lambda}{q_e^2}. \end{aligned} \tag{26}$$

Replacing the above relation into Eq. (23), ΔG_e can be expressed in a final simple closed form as

$$\begin{aligned} \Delta G_e &= \frac{2\mathrm{j}nk_e}{n+1}\int_0^\infty J_0(\lambda r)\mathrm{e}^{-\mathrm{j}q_e(z+H)}\frac{\lambda}{q_e^2}\mathrm{d}\lambda \\ &= -\frac{2\mathrm{j}nk_e}{n+1}I(r,R_2), \end{aligned} \tag{27}$$

where by defining a new variable of integration, ζ, the right-hand side of this equation can be written as (Tokarsky and Dolzhikov, 1998)

$$\begin{aligned} I(r,R_2) &= \int_0^\infty J_0(\lambda r)\mathrm{e}^{-\mathrm{j}\sqrt{k_e^2-\lambda^2}(z+H)}\frac{\lambda}{\lambda^2-k_e^2}\mathrm{d}\lambda \\ &= \int_1^\infty \frac{\mathrm{e}^{-\mathrm{j}k_e R_2\zeta}}{\sqrt{\zeta^2-(r/R_2)^2}}\mathrm{d}\zeta. \end{aligned} \tag{28}$$

Finally, the following relation can introduce the numerical solution for the above integral:

$$I(r,R_2)=\sum_{m=0}^{\infty}A_m T_{2m+1}(\mathrm{j}k_e R_2), \tag{29}$$

where A_m, $T_{2m+1}(\mathrm{j}k_e R_2)$, and R_2 are as introduced in Appendix C.

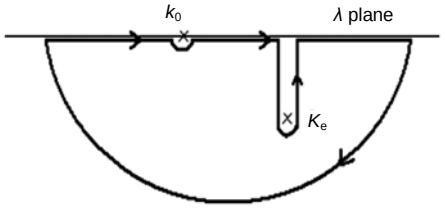

Fig. 4 Contour for Eq. (25) and representation of branch points

3 Modeling the soil ionization

One important aspect in grounding system simulation is the soil ionization modeling. When a high magnitude current is leaked into the earth, soil ionization will occur if this current exceeds a critical value. The grounding conductor will then be surrounded by a cylindrical volume of ionized soil (corona type discharge), and in this region the voltage drop can be considered negligible. This phenomenon is modeled by increasing the equivalent radius of the grounding conductors (Zhang *et al.*, 2005).

The critical value of the electric field intensity for the soil to be ionized, E_{crit}, is a function of earth conductivity, and is obtained by the empirical formula (Mentre and Grcev, 1994) as follows:

$$E_{crit}=241\sigma_e^{-0.215}\ \text{kV/m}. \tag{30}$$

Given that the soil ionization effect and the comparison between the electric field value with the above critical value should be performed in the time domain, the soil ionization modeling stage is placed after the computation in the frequency domain is completed and transformed to the time domain, i.e., whenever the electric field and voltage at the desired point and at time t are calculated.

Therefore, after computing the leakage current I_ℓ from Eq. (9), the normal electric field on the surface of each segment in the frequency domain can be obtained by Ohm's law, i.e.,

$$\boldsymbol{E}=\frac{\boldsymbol{I}_\ell}{2\pi r(\sigma_e+\mathrm{j}\omega\varepsilon_e)\ell_{seg}}\times10^{-3}\ \text{kV/m}, \tag{31}$$

where r is the radius of the grounding conductor and ℓ_{seg} is the length of each segment of the grounding system.

Then, by using the FILT algorithm (refer to Eqs. (33) to (36)), the electric field in the time domain, $\tilde{E}$, is calculated. Finally, the effective radius for each segment of the grounding conductor, r_{eff}, can be computed by (whenever $\tilde{E}$ becomes greater than E_{crit}) (Cidras *et al.*, 2000)

$$r_{eff}=r\frac{\tilde{E}}{E_{crit}}. \tag{32}$$

Consequently, whenever the soil ionization effect should be considered, for any segment, its physical radius is substituted by r_{eff}. The computed radii are used in the next time step (or iteration) of calculation.

4 The proposed procedure

In the proposed method for computing the transient voltage at any point, near or far from a grounding electrode (or in a wider sense, a grid), the following steps are performed:

Step 1: Computation of the impedance matrix, $\boldsymbol{Z}$, from Eq. (17), at each specified frequency.

Step 2: Computation of the impedance vector, $\boldsymbol{Z}_{\text{s}}$, from Eq. (18), at each specified frequency.

Step 3: Calculation of leakage current of each segment, from Eq. (9), at each specified frequency.

Step 4: Computation of the voltage at the desired point (as the sum of the two components, introduced in Eqs. (7) and (8)).

Step 5: Performing all of the above steps at the specified frequencies for applying fast inverse Laplace transform (refer to the next section), and calculating the time-domain responses.

Step 6: Checking for soil ionization in all segments and correcting the relevant elements of $\boldsymbol{Z}$ to be used in the next time step.

Step 7: Moving to the next time step and performing Steps 1–6 while assigning the relevant set of frequencies for the FILT operation.

5 Fast inverse Laplace transform

For the time domain conversion of any function in the Laplace domain, $F(s)$, the following well-known relation is used:

$$f(t)=\frac{1}{2\pi \mathrm{j}}\int_{\gamma-\mathrm{j}\infty}^{\gamma+\mathrm{j}\infty}F(s)\mathrm{e}^{st}\,\mathrm{d}s. \tag{33}$$

The above integral may be solved, analytically, for only some particular forms of $F(s)$. It is possible, however, to solve it through numerical methods. According to Hosono (1981), the following relation can be used to calculate $f(t)$ numerically:

$$f^{\ell m}(t)=\frac{\mathrm{e}^{a}}{t}\left(\sum_{n=1}^{\ell-1}F_n+2^{-m-1}\sum_{n=0}^{m}A_{mn}F_{\ell+n}\right), \tag{34}$$

where

$$F_n=(-1)^n\,\mathrm{Im}\left\{F\{[a+\mathrm{j}(n-0.5)\pi]/t\}\right\}, \tag{35}$$

and

$$A_{mm}=1,\ A_{mn-1}=A_{mn}+\binom{m+1}{n}. \tag{36}$$

The first step for computing the inverse Laplace transform is to choose properly the parameters a, m, and ℓ to be placed into Eq. (34). Extensive inspection for applying FILT in the high frequency analysis of grounding systems has resulted in assigning a=2, m=10, and $\ell=15$.

Note that according to Eq. (35), $[a+\mathrm{j}(n-0.5)\pi]/t$ represents the set of frequencies at which F should be calculated to compute $f(t)$.

6 Results and discussion

To verify the results obtained using the proposed method, we compared them with the published results for similar grounding systems. Also, the results after considering soil ionization and changing the position of the feed point on the frequency response of the grounding system are presented.

6.1 Validation of the proposed method

To evaluate the validity of the proposed method, three strategies have been designed. The first strategy is to compare the correction term (ΔG_{e}) of the proposed method, i.e., Eq. (27), and the approximate method in Poljak and Doric (2006). The second is to evaluate the integrand of the integral Eq. (26) and the exact integrand of Eq. (24). The last strategy is to compare the obtained frequency response of the input impedance for the grounding electrode by the proposed method versus the aforementioned methods.

6.1.1 Comparison between the results of ΔG_{e}

Fig. 5 shows the results for ΔG_{e} by the proposed method and the approximate procedure in Poljak and Doric (2006). The results are in good agreement for the far distances between the observation point and the grounding electrode. For the case of near distances, however, the results of the approximate procedure deviate from those of the proposed method.

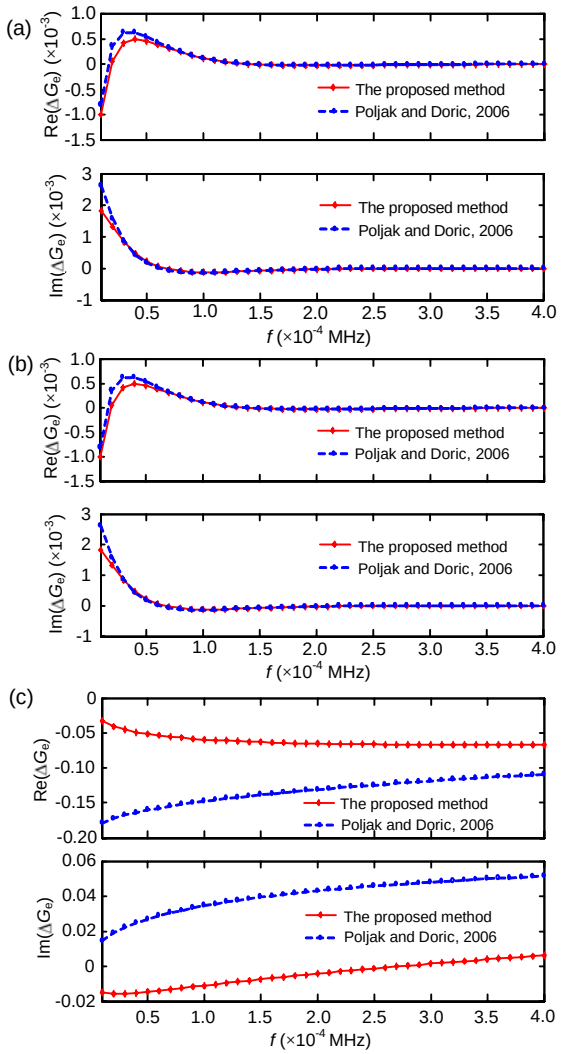

Fig. 5 Comparison between the results of ΔG_e in different observation points: (a) r=500 m; (b) r=200 m; (c) r=10 m

6.1.2 Comparison between the integrand values

By defining a normalized variable as $X=\lambda/k_0$, the original integrand of SI in Eq. (24), the proposed integrand in Eq. (26) and the approximate method, named as the reflection coefficient method in Ishimaru (1991), can be represented by the following relations.

1. The original integrand

The integrand of Eq. (24) as a function of X can be rewritten as

$$F_{\text{exact}}=\frac{2\mathrm{j}k_e^2X\sqrt{1-X^2}}{nk_e\sqrt{1-X^2}+k_0\sqrt{n^2-X^2}}\frac{\mathrm{e}^{-\mathrm{j}k_0\sqrt{n^2-X^2}(z+H)}}{k_0\sqrt{n^2-X^2}}J_0(k_0rX). \quad (37)$$

2. The proposed integrand

According to the proposed method, the relevant integrand in Eq. (26) is changed to the following relation:

$$F_{\text{proposed}}=\frac{2\mathrm{j}nk_e}{n+1}\frac{X}{k_0(n^2-X^2)}\mathrm{e}^{-\mathrm{j}q_e(z+H)}J_0(k_0rX). \quad (38)$$

3. Approximate integrand

According to Harrington (2001), the Bessel function in the integrand of SI is approximated by $J_0(\lambda r)=\sqrt{2/(\pi\lambda r)}\cos(\lambda r-\pi/4)$ for large arguments. Consequently, the related integrand can be stated by the following relation, which is valid for the far-field calculation:

$$F_{\text{approximate}}=\frac{2\mathrm{j}k_e^2X\sqrt{1-X^2}}{nk_e\sqrt{1-X^2}+k_0\sqrt{n^2-X^2}}\frac{\mathrm{e}^{-\mathrm{j}k_0\sqrt{n^2-X^2}(z+H)}}{k_0\sqrt{n^2-X^2}}\cdot\sqrt{\frac{2}{\pi k_0rX}}\cos\left(k_0rX-\frac{\pi}{4}\right). \quad (39)$$

Fig. 6 shows the integrand values of the three procedures for different distances between the observation points and the grounding electrode and also various frequencies (100 kHz and 3 MHz). As is shown, the results of the proposed method are in good agreement with the exact integrand, particularly for the near distances.

6.1.3 Comparison between the input impedances

Due to the data and the results of the models presented in Grcev (1986), Doric *et al.* (2004), and Shahrtash and Ramezani (2008), which were available for a horizontal electrode with the following data, the proposed method in this study is also applied to the same system.

The grounding system consists of a horizontal electrode, with length L=1 m, radius r=5 mm, buried at the depth of H=1 m, where the soil parameters are $\varepsilon_e=8.85\times10^{-11}$ and $\mu_e=4\pi\times10^{-7}$ with two different conductivities as σ_e=0.001 and 0.01 s/m. A double exponential current source, $I_s=1.1043\times(\mathrm{e}^{-0.07924\times10^6t}-\mathrm{e}^{-4.0011\times10^6t})$, is injected to the left end of this electrode.

The frequency response of the input impedance for the mentioned horizontal grounding electrode is

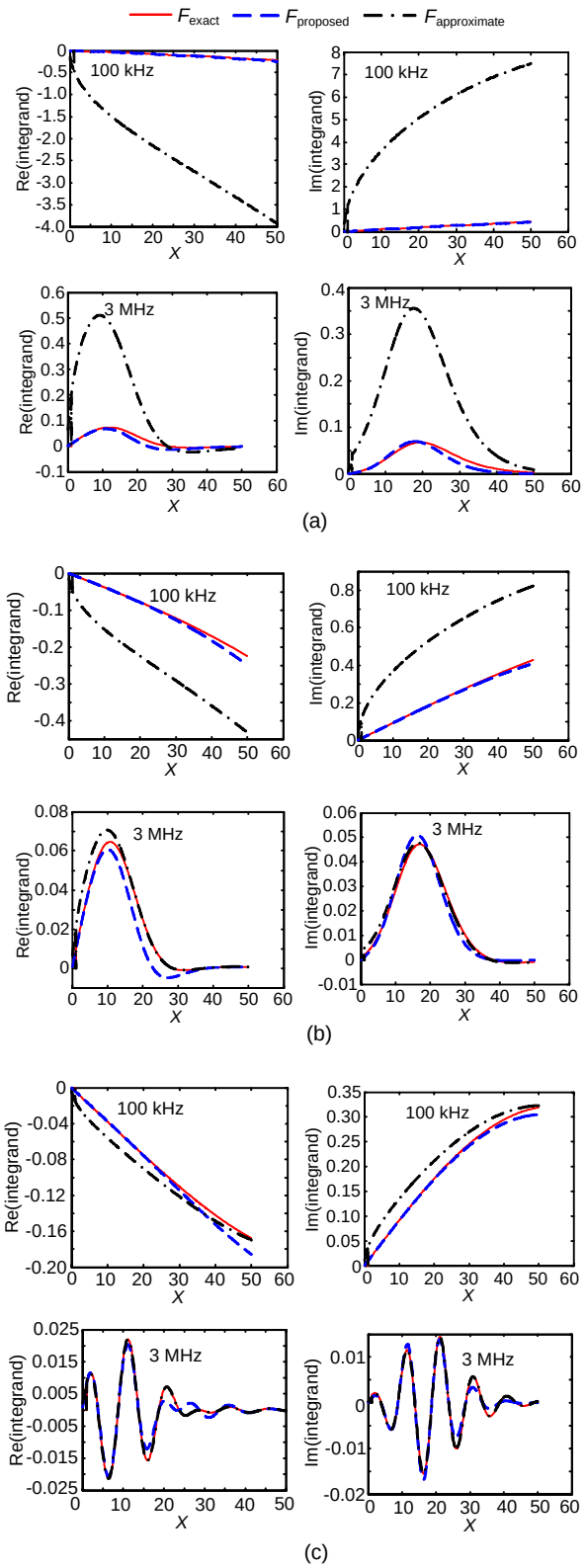

Fig. 6 Comparison between the results of integrand in different distances and various frequencies: (a) r=0.01 m; (b) r=1 m; (c) r=10 m

shown in Fig. 7, which is a comparison among the results of the proposed method and the mentioned references.

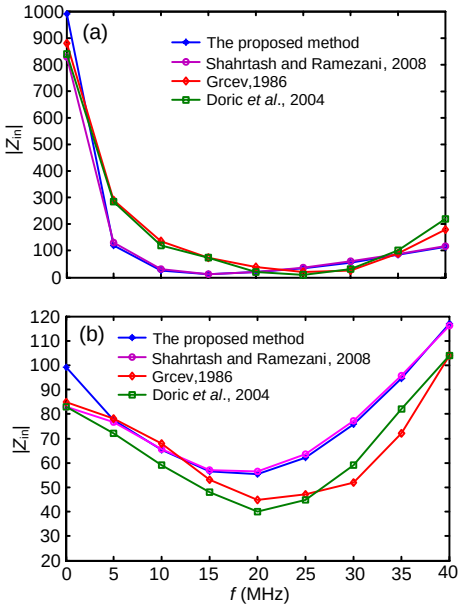

Fig. 7 Input impedance of the grounding electrode
(a) σ_e=0.001 s/m; (b) σ_e=0.01 s/m

As depicted, when the approximations that are valid only for the far fields are applied in computing the cases of near fields, as was done in Grcev (1986), Doric *et al.* (2004), and Shahrtash and Ramezani (2008), some large deviations from the results of the proposed method are found; but, the overall trends are similar and there is good agreement. It is worth mentioning that far-field approximation is valid only for computing the scalar potential at the points that are farther than $2D^2/\lambda$ from the grounding electrode (D is the length of each segment and λ is the smallest wavelength of the considered frequency spectrum) (Stutzman and Thiele, 1997).

6.2 Time domain response

In this subsection, transient voltages are calculated in the time domain at the feed point and at the center of the same grounding electrode. The results are obtained using the FILT procedure.

The transient voltages show considerable attenuation and distortion, by decreasing in the slope of the wavefront as shown in the rightmost curves in Fig. 8, along the grounding electrode in both cases.

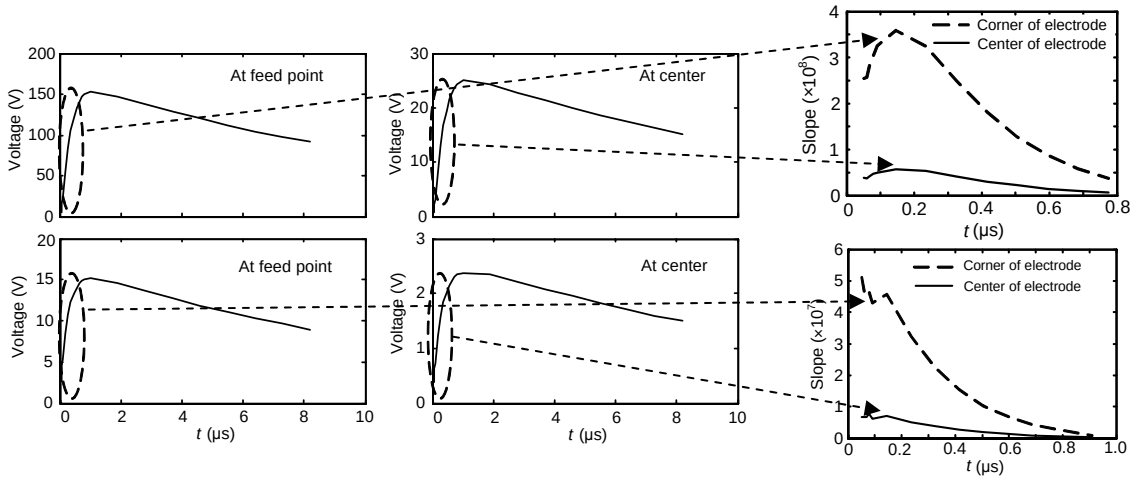

Fig. 8 Transient voltages at the surface of the grounding electrode for σ_e=0.001 s/m (top) and σ_e=0.01 s/m (bottom)

6.3 Influence of the location of the feed point

Fig. 9 shows the result of the proposed method for a grounding system with the size of 1 m×1 m and four meshes. Two cases were studied and the results are shown, one where the feed point is at the corner and the other at the center of the grounding grid. As shown, the input impedance in the former case is higher than in the latter one.

6.4 Influence of soil ionization

The transient responses with and without the soil ionization model are shown for the electrode in Section 6.1.3 (Fig. 10), while a double exponential current source with a magnitude of 500 A was considered. As shown, soil ionization results in a lower magnitude for the transient ground potential rise (TGPR) of the grounding electrode.

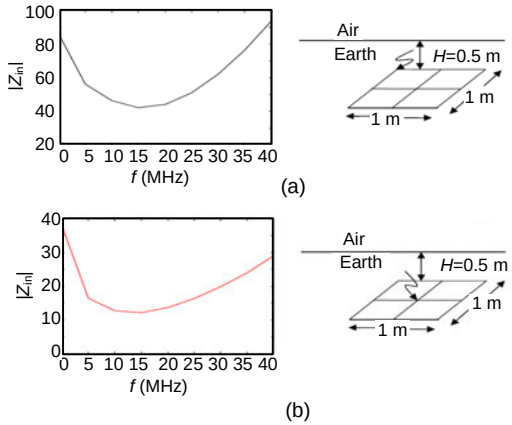

Fig. 9 Input impedance of the grounding system for different feed points at the corner (a) and the center (b)

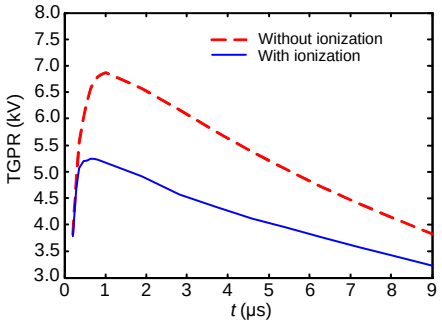

Fig. 10 Transient ground potential rise (TGPR) for the grounding electrode with and without soil ionization

7 Conclusions

In this paper, a unified, novel, and electromagnetic field based approach is proposed to analyze the high frequency behavior of the grounding grid. This numerical method computes the leakage currents of each segment of the grounding system with the method of moments (MOM). The main feature of the presented method is that it is based on solving the full set of Maxwell's equations with developing suitable closed-form relations for computing the Green function. These simple and accurate expressions are substituted, instead of the rigorous Sommerfeld integrals, for considering the influence of the half-space interface (air/earth).

The method is valid for a wide range of frequencies and is able to calculate the electromagnetic fields not only in far points, but also at near distances with respect to the grounding electrode. The transient

voltages in the time domain can be calculated at any desired point by fast inverse Laplace transform. Moreover, the soil ionization phenomenon is easily included in the proposed procedure.

Finally, different results from the proposed method are obtained and compared with those obtained using the published procedures, wherein good agreement is observed.

References

Andolfato, R., Bernardi, L., Fellin, L., 2000. Aerial and grounding systems analysis by the shifting complex images method. *IEEE Trans. Power Del.*, **15**(3):1001-1009. [doi:10.1109/61.871366]

Arnautovski-Toseva, V., Grcev, L., 2004. Electromagnetic analysis of horizontal wire in two-layered soil. *J. Comput. Appl. Math.*, **168**(1-2):21-29. [doi:10.1016/j.cam.2003.05.014]

Cidras, J., Otero, A.F., Garrido, C., 2000. Nodal frequency analysis of grounding systems considering the soil ionization effect. *IEEE Trans. Power Del.*, **15**(1):103-107. [doi:10.1109/61.847236]

Doric, V., Poljak, D., Roje, V., 2004. Transient analysis of the grounding electrode based on the wire antenna theory. *Eng. Anal. Bound. Elem.*, **28**(7):801-807. [doi:10.1016/j.enganabound.2003.11.001]

Gao, Y.Q., He, J.L., Zeng, R., Liang, X.D., 2002. Impulse Transient Characteristic of Grounding Grid. 3rd Int. Symp. on Electromagnetic, p.276-280. [doi:10.1109/ELMAGC.2002.1179385]

Geri, A., 1999. Behavior of ground systems excited by high impulse currents: the model and its validation. *IEEE Trans. Power Del.*, **14**(3):1008-1017. [doi:10.1109/61.772347]

Geri, A., Veca, G.M., Garbagnati, E., Sartorio, G., 1992. Nonlinear behavior of ground electrodes under lightning surge currents: computer modeling and comparison with experimental results. *IEEE Trans. Magn.*, **28**(2):1442-1445. [doi:10.1109/20.123966]

Grcev, L., 1986. Calculation of the Transient Impedance of Grounding Systems. PhD Thesis, University of Zagreb, Croatian.

Harrington, R.F., 2001. Time-Harmonic Electromagnetic Fields. Wiley-IEEE Press.

Heimbach, M., Grcev, L.D., 1997. Grounding system analysis in transients programs applying electromagnetic field approach. *IEEE Trans. Power Del.*, **12**(1):186-193. [doi:10.1109/61.568240]

Hosono, T., 1981. Numerical inversion of Laplace transform and some applications to wave optics. *Radio Sci.*, **16**(6):1015-1019. [doi:10.1029/RS016i006p01015]

Ishimaru, A., 1991. Electromagnetic Wave Propagation, Radiation, and Scattering. Prentice-Hall Inc., Englewood Cliffs, NJ.

Liu, Y.Q., Zitnik, M., Thottappillil, R., 2001. An improved transmission line model of grounding systems. *IEEE Trans. Electromagn. Compat.*, **43**(3):348-355. [doi:10.1109/15.942606]

Lorentzou, M.I., Hatziargyriou, M.I., Papadias, N.D., 2003. Time domain analysis of grounding electrodes impulse response. *IEEE Trans. Power Del.*, **18**(2):517-524. [doi:10.1109/TPWRD.2003.809686]

McAllister, I.W., Crichton, G.C., 1991. Analysis of the temporal electric fields in lossy dielectric media. *IEEE Trans. Electr. Insul.*, **26**(3):513-528. [doi:10.1109/14.85125]

Meliopoulos, A.P., Moharam, M.G., 1983. Transient analysis of grounding systems. *IEEE Trans. Power Appar. Syst.*, **102**(2):389-399. [doi:10.1109/TPAS.1983.317686]

Mentre, F.E., Grcev, L., 1994. EMTP-based model for grounding system analysis. *IEEE Trans. Power Del.*, **9**(4):1838-1849. [doi:10.1109/61.329517]

Otero, A.F., Cidras, J., del Alamo, J.L., 1999. Frequency-dependence grounding system calculation by means of a conventional nodal analysis technique. *IEEE Trans. Power Del.*, **14**(3):873-878. [doi:10.1109/61.772327]

Poljak, D., Doric, V., 2006. Wire antenna model for transient analysis of simple grounding systems, part I: the vertical grounding electrode. *Progr. Electromagn. Res.*, **64**:149-166. [doi:10.2528/PIER06062101]

Portela, C., 1997. Frequency and Transient Behavior of Grounding Systems, Part I. Physical and Methodological Aspects. IEEE Int. Symp. on Electromagnetic Compatibility, p.379-384.

Ramamoorty, M., Babu Narayanan, M.M., Parameswaran, S., Mukhedkar, D., 1989. Transient performance of grounding grids. *IEEE Trans. Power Del.*, **4**(4):2053-2059. [doi:10.1109/61.35630]

Shahrtash, S.M., Ramezani, N., 2008. A New Approach to Compute Transient Behavior of Grounding Electrodes in Time-Domain. Joint Int. Conf. on Power System Technology and IEEE Power India Conf., p.1-5. [doi:10.1109/ICPST.2008.4745321]

Stutzman, W.L., Thiele, G.A., 1997. Antenna Theory and Design. Wiley, New York.

Tokarsky, P.L., Dolzhikov, V.V., 1998. Simple Approximate Formulas for Evaluating Sommerfeld Type Integrals. VIIth Int. Conf. on Mathematical Methods in Electromagnetic Theory, p.246-248.

Velazquez, R., Mukhedkar, D., 1984. Analytical modeling of grounding electrodes transient behavior. *IEEE Trans. Power Appar. Syst.*, **103**(6):1314-1322. [doi:10.1109/TPAS.1984.318465]

Verma, R., Mukhedkar, D., 1980. Impulse impedance of buried ground wire. *IEEE Trans. Power Appar. Syst.*, **99**(5):2003-2007. [doi:10.1109/TPAS.1980.319827]

Zhang, B., He, J., Lee, J., Cui, X., Zhao, Z., Zou, J., Chang, S., 2005. Numerical analysis of transient performance of grounding systems considering soil ionization by coupling moment method with circuit theory. *IEEE Trans. Magn.*, **41**(5):1440-1443. [doi:10.1109/TMAG.2005.844547]

Appendix A: the magnetic vector potential

According to Maxwell's law, the divergence of magnetic field density $\boldsymbol{B}$ is zero and, in general the divergence of the curl of any vector is zero. Thus, $\boldsymbol{B}$ can be expressed by the curl of an arbitrary vector $\boldsymbol{A}$, called the magnetic vector potential:

$$\nabla \cdot \boldsymbol{B} = 0, \tag{A1}$$

$$\boldsymbol{B} = \nabla \times \boldsymbol{A}. \tag{A2}$$

Using the Biot-Savart law, the magnetic field caused by a volume current density $\boldsymbol{J}_\ell$ is calculated by

$$\boldsymbol{B} = \int_{v'} \frac{\mu_0 \boldsymbol{J}_\ell(\boldsymbol{R}') \times (\boldsymbol{R} - \boldsymbol{R}')}{4\pi \left| \boldsymbol{R} - \boldsymbol{R}' \right|^3} \mathrm{d}v'. \tag{A3}$$

In addition,

$$\nabla \frac{1}{\left| \boldsymbol{R} - \boldsymbol{R}' \right|} = -\frac{\boldsymbol{R} - \boldsymbol{R}'}{\left| \boldsymbol{R} - \boldsymbol{R}' \right|^3}. \tag{A4}$$

Therefore,

$$\boldsymbol{B} = \frac{\mu_0}{4\pi} \int_{v'} \left[-\boldsymbol{J}_\ell(\boldsymbol{R}') \times \nabla \frac{1}{\left| \boldsymbol{R} - \boldsymbol{R}' \right|} \right] \mathrm{d}v'. \tag{A5}$$

Also, according to the following relation:

$$\nabla \times (\boldsymbol{f} \cdot \boldsymbol{F}) = \boldsymbol{f} \cdot \nabla \times \boldsymbol{F} - \boldsymbol{F} \times \nabla \cdot \boldsymbol{f}, \tag{A6}$$

Eq. (A5) can be substituted by

$$\nabla \times \frac{\boldsymbol{J}_\ell(\boldsymbol{R}')}{\left| \boldsymbol{R} - \boldsymbol{R}' \right|} = \frac{1}{\left| \boldsymbol{R} - \boldsymbol{R}' \right|} \nabla \times \boldsymbol{J}_\ell(\boldsymbol{R}') - \boldsymbol{J}_\ell(\boldsymbol{R}') \times \nabla \frac{1}{\left| \boldsymbol{R} - \boldsymbol{R}' \right|}. \tag{A7}$$

Since $\boldsymbol{J}_\ell(\boldsymbol{R}')$ is not a function of $\boldsymbol{R}$, thus,

$$\nabla \times \boldsymbol{J}_\ell(\boldsymbol{R}') = \boldsymbol{0}. \tag{A8}$$

Consequently,

$$\boldsymbol{B} = \frac{\mu_0}{4\pi} \int_{v'} \nabla \times \frac{\boldsymbol{J}_\ell(\boldsymbol{R}')}{\left| \boldsymbol{R} - \boldsymbol{R}' \right|} \mathrm{d}v' = \frac{\mu_0}{4\pi} \nabla \times \int_{v'} \frac{\boldsymbol{J}_\ell(\boldsymbol{R}')}{\left| \boldsymbol{R} - \boldsymbol{R}' \right|} \mathrm{d}v'. \tag{A9}$$

Comparing Eq. (A2) with Eq. (A9), it can be concluded that

$$\boldsymbol{A} = \frac{\mu_0}{4\pi} \int_{v'} \frac{\boldsymbol{J}_\ell(\boldsymbol{R}')}{\left| \boldsymbol{R} - \boldsymbol{R}' \right|} \mathrm{d}v'. \tag{A10}$$

For an electric source buried into the earth with the permeability of μ_e, Eq. (A10) can be converted to

$$\boldsymbol{A} = \frac{\mu_\mathrm{e}}{4\pi} \int_{v'} \frac{\boldsymbol{J}_\ell(\boldsymbol{R}')}{\left| \boldsymbol{R} - \boldsymbol{R}' \right|} \mathrm{d}v'. \tag{A11}$$

Appendix B: the voltage at any point

Assuming that a leakage current, I_ℓ, drains into the soil, the volume leakage current density, $\boldsymbol{J}_\ell$, is computed, according to the image theory, by

$$\boldsymbol{J}_\mathrm{e}(v) = \frac{I_\ell}{4\pi} \left(\frac{1}{r^2} \boldsymbol{r} + \frac{1}{r'^2} \boldsymbol{r}' \right), \tag{B1}$$

where r and r' are the distances between the current leakage point and its image from the observation point, respectively.

Therefore, the scattered field is obtained by substituting Eq. (B1) into Eq. (11):

$$\boldsymbol{E}_\mathrm{s}(r, \omega) = \frac{I_\ell}{4\pi(\sigma_\mathrm{e} + \mathrm{j}\omega\varepsilon_\mathrm{e})} \left(\frac{1}{r^2} \boldsymbol{r} + \frac{1}{r'^2} \boldsymbol{r}' \right). \tag{B2}$$

Also, according to Eq. (13), for any leakage current, the vector potential at any observation point in space can be calculated by

$$\boldsymbol{A}(r) = \frac{\mu_\mathrm{e} I_\ell}{4\pi} \left(\frac{1}{r^2} \boldsymbol{r} + \frac{1}{r'^2} \boldsymbol{r}' \right). \tag{B3}$$

As the induced voltage at that observation point can be calculated by Eq. (12) consequently through the following relation:

$$\nabla V = -(\boldsymbol{E}_\mathrm{s} + \mathrm{j}\omega \boldsymbol{A}), \tag{B4}$$

by using Eqs. (B2) and (B4), the voltage at the observation point can be found:

$$\begin{aligned} V_P(r, \mathrm{j}\omega) &= \int_r^\infty E_\mathrm{s}(r, \mathrm{j}\omega) \mathrm{d}r + \mathrm{j}\omega \int_r^\infty A(r) \mathrm{d}r \\ &= \frac{I}{4\pi} \left(\frac{1}{\sigma_\mathrm{e} + \mathrm{j}\omega\varepsilon_\mathrm{e}} + \mathrm{j}\omega\mu_\mathrm{e} \right) \left(\frac{1}{r} + \frac{1}{r'} \right). \end{aligned} \tag{B5}$$

As shown in Fig. B1, where a grounding conductor contains a number of above current leakage points (i.e., the current segments), the induced voltage at P is obtained by

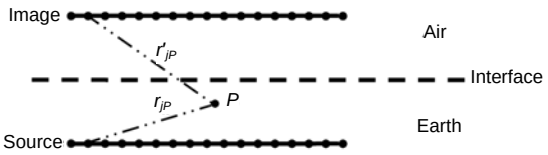

Fig. B1 A grounding conductor representing a number of current leakage points

$$V_P(r,\mathrm{j}\omega)=\frac{1}{4\pi}\left(\frac{1}{\sigma_\mathrm{e}+\mathrm{j}\omega\varepsilon_\mathrm{e}}+\mathrm{j}\omega\mu_\mathrm{e}\right)\sum_{j=1}^{k}\left(\frac{I_j}{r_{jP}}+\frac{I'_j}{r'_{jP}}\right). \quad \text{(B6)}$$

Assuming a uniform leakage current density for all of the segments, such as

$$\frac{I_j}{\Delta x}=\frac{I}{L}=J_\ell, \quad \text{(B7)}$$

where Δx is the length of the segment and L is the total length of the conductor, Eq. (B6) can be converted to

$$V_P(r,\mathrm{j}\omega)=\frac{1}{4\pi}\left(\frac{1}{\sigma_\mathrm{e}+\mathrm{j}\omega\varepsilon_\mathrm{e}}+\mathrm{j}\omega\mu_\mathrm{e}\right)\int_0^L J_\ell\left(\frac{1}{r_{jP}}+\frac{1}{r'_{jP}}\right)\mathrm{d}x. \quad \text{(B8)}$$

In high frequency analysis, Eq. (B8) can be replaced by

$$V_P(r,\mathrm{j}\omega)=\frac{1}{4\pi}\left(\frac{1}{\sigma_\mathrm{e}+\mathrm{j}\omega\varepsilon_\mathrm{e}}+\mathrm{j}\omega\mu_\mathrm{e}\right)\int_0^L J_\ell(\ell_n)G(r_m)\mathrm{d}\ell_n, \quad \text{(B9)}$$

where $G(r_m)$ for high frequency analysis is described in the text.

Appendix C: numerical solution of the Sommerfeld type integral for a vertical electric dipole above the earth

According to Tokarsky and Dolzhikov (1998), the Green function can be calculated for a vertical electric dipole, located above a lossy half-space as follows:

$$G(\boldsymbol{r})=\frac{\mathrm{e}^{-\mathrm{j}k_0R_1}}{R_1}+\frac{\mathrm{e}^{-\mathrm{j}k_0R_2}}{R_2}+\int_0^\infty\frac{-2k_0^2q_\mathrm{e}}{k_\mathrm{e}^2q_0+k_0^2q_\mathrm{e}}\frac{\lambda}{q_0}J_0(\lambda r)\mathrm{e}^{-q_0(z+H)}\mathrm{d}\lambda, \quad \text{(C1)}$$

$$G(\boldsymbol{r})=G(R_1)+G(R_2)+\Delta G, \quad \text{(C2)}$$

where $G(R_1)$ and $G(R_2)$ are the Green functions in the free space. In addition, the correction term due to the existence of the air/earth medium interface, ΔG, can be written as

$$\Delta G=\int_0^\infty f(\lambda)J_0(\lambda r)\mathrm{e}^{-q_0(z+H)}\mathrm{d}\lambda, \quad \text{(C3)}$$

where

$$R_1=\sqrt{r^2+(z-H)^2},\quad R_2=\sqrt{r^2+(z+H)^2},\quad q_0=\sqrt{\lambda^2-k_0^2},\quad q_\mathrm{e}=\sqrt{\lambda^2-k_\mathrm{e}^2}, \quad \text{(C4)}$$

and $f(\lambda)$ is

$$f(\lambda)=\frac{-2k_0^2}{k_\mathrm{e}^2q_0+k_0^2q_\mathrm{e}}\frac{\lambda}{q_0}. \quad \text{(C5)}$$

Then, by substituting Eq. (C5) in Eq. (C3), the final relation for ΔG can be represented as (by defining $n=k_\mathrm{e}/k_0$)

$$\Delta G\approx-\mathrm{j}\frac{2k_0}{n+1}I(r,R_2). \quad \text{(C6)}$$

On the other hand, a numerical solution exists for $I(r, R_2)$, which is

$$I(r,R_2)=\sum_{m=0}^{\infty}A_mT_{2m+1}(\mathrm{j}k_0R_2),\quad m\in\mathbb{Z}. \quad \text{(C7)}$$

In the above relation, the related parameters can be obtained by the following formulas:

$$T_{2m+1}(\mathrm{j}kR)=\frac{\mathrm{e}^{-\mathrm{j}kR}}{2m}\left(1-\frac{\mathrm{j}kR}{2m-1}\right)-\frac{(kR)^2}{2m(2m-1)}T_{2m-1}(\mathrm{j}kR), \quad \text{(C8)}$$

$$A_m=\frac{2m-1}{2m}\frac{r}{R_2}A_{m-1},\quad A_0=1, \quad \text{(C9)}$$

$$T_1(\mathrm{j}kR)=-\gamma-\ln(\mathrm{j}kR)-\sum_{n=1}^{\infty}\frac{(-1)^n(\mathrm{j}kR)^n}{n\cdot n!},\quad \gamma=0.577\,215\,664\,9. \quad \text{(C10)}$$

Finally, by using Eq. (C7), the solution for ΔG, an SI type function, is found through Eq. (C6).